ACS APPLIED MATERIALS & INTERFACES

Research Article

www.acsami.org

Effect of AIE Substituents on the Fluorescence of Tetraphenylethene-Containing BODIPY Derivatives

Cesar F. Azael Gomez-Duran,[†] Rongrong Hu,[†,∥] Guangxue Feng,[§] Tingzhong Li,[∥] Fan Bu,[∥] Mathieu Arseneault,[†] Bin Liu,*[,§] Eduardo Peña-Cabrera,*[,‡] and Ben Zhong Tang*[,†,∥,⊥]

[†]Department of Chemistry, Institute for Advanced Study, Institute of Molecular Functional Materials, Division of Biomedical Engineering, Division of Life Science, and State Key Laboratory of Molecular Neuroscience, The Hong Kong University of Science & Technology (HKUST), Clear Water Bay, Kowloon, Hong Kong

[‡]Departamento de Química, Universidad de Guanajuato, Col. Noria Alta S/N, Guanajuato, Guanajuato 36050, Mexico

[§]Department of Chemical and Biomolecular Engineering, National University of Singapore, 4 Engineering Drive 4, 117585, Singapore

[∥]Guangdong Innovative Research Team, SCUT-HKUST Joint Research Laboratory, State Key Laboratory of Luminescent Materials and Devices, South China University of Technology (SCUT), Guangzhou 510640, China

[⊥]HKUST-Shenzhen Research Institute, No. 9 Yuexing First RD, South Area, Hi-Tech Park, Nanshan, Shenzhen 518057, China

Supporting Information

ABSTRACT: A series of BODIPY derivatives with tetraphenylethene (TPE) moieties were designed and synthesized. The effect of positions and numbers of substitution groups on the fluorescence of the BODIPYs was investigated. Theoretical calculation and single crystal structures proved that the TPE substitution groups on the 8-position of BODIPY contributed little to the conjugation, but benefited the aggregated state emission. On the other hand, the substitutions on the 3- or 5-position of BODIPY through vinyl bridges increased the conjugation length, and generated big coplanar π-conjugated structures with poor aggregated state emission. The compound with bright aggregated state emission has been further fabricated into biocompatible fluorescent nanoparticles and used as effective fluorescent contrast agents for intracellular imaging.

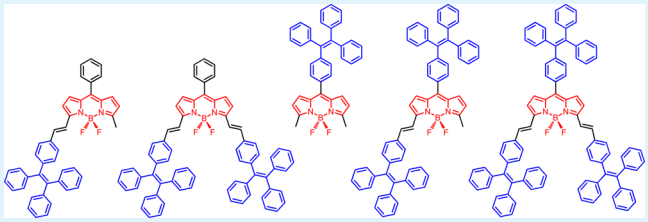

KEYWORDS: *aggregation-induced emission, BODIPY, tetraphenylethene, substitution effect, cellular imaging*

INTRODUCTION

The development of red or NIR emitters is in urgent demand because of the deep penetration depth and low autofluorescence from biosubstrates in the red or NIR region.[1,2] Among numerous organic fluorescent dyes, borondipyrromethene (BODIPY) derivatives have received much research interest due to abundant advantages such as narrow emission spectra, high fluorescence quantum yields, large absorption coefficients and two-photon cross sections, excellent photo/chemostability, easy modification, and structural varieties.[3] They have been reported to serve as fluorescent probes, sensors, and switches, as well as light harvesting antennas and solar cell sensitizers.[4−6] In particular, they are widely used in biological sensing and imaging for mitochondrial copper detection, DNA labeling, live cell glucagon imaging, or polymerase chain reaction.[7,8] Extensive reviews have described their synthesis, properties, and applications.[9,10] However, BODIPY dyes and their derivatives also have obvious disadvantages, such as aggregation-caused quenching (ACQ) effect and small Stokes shift, which have limited their further development.[11,12]

To solve the notorious ACQ problem of many widely used fluorescent dyes, an aggregation-induced emission (AIE) phenomenon was reported in a series of propeller-shaped molecules such as tetraphenylethene (TPE).[13−16] AIE compounds normally show no obvious emission in solution, but emit intensely in aggregated states.[17] Mechanistic studies suggested that the restriction of intramolecular motions, including rotation and vibration, in the aggregated or other condensed state was the main reason for AIE effect.[18] The attachment of AIE moieties to traditional ACQ dyes can also successfully transform them into AIE compounds with desirable aggregated state emission.[19]

A few works have been reported marrying BODIPY and AIE moieties in a single molecule to generate AIE-active BODIPYs with large Stokes shifts. For example, BODIPYs carrying triphenylamine units show both twisted intramolecular charge transfer (TICT) and AIE characteristics. In polar solvents, the luminogens turn from the locally excited (LE) state to the TICT state through intramolecular rotation, bringing about a TICT emission peak at longer wavelength compared with the LE emission, and result in large Stokes shift. This TICT peak is further enhanced in the aggregated state, demonstrating AIE effect.[20] Three TPE-BODIPY hybrids with C—C (TPB), C═C (TPVB), and C≡C bonds (TPEB) connecting TPE and

Received: December 23, 2014
Accepted: June 25, 2015
Published: June 25, 2015

DOI: 10.1021/acsami.5b05033
ACS Appl. Mater. Interfaces 2015, 7, 15168−15176

Chart 1. Chemical Structures of Compounds 1−5

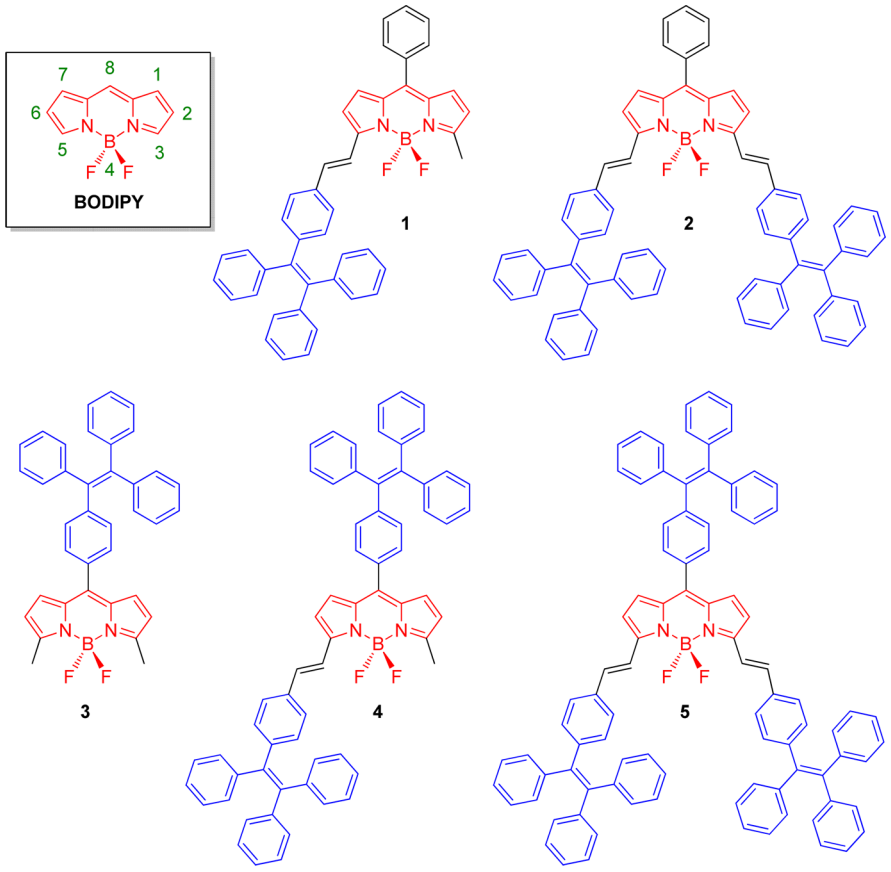

Scheme 1. Synthetic Routes towards Compounds 1−5

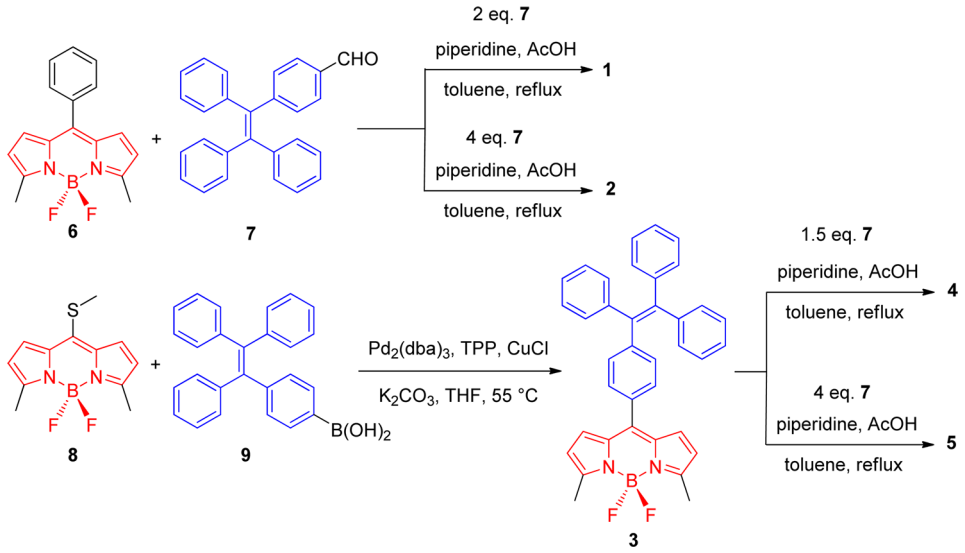

BODIPY units were synthesized to study the conjugation effect on the aggregated state emission. TPB only has an ACQ-active LE emission peak, and TPVB with best conjugation has an AIE-active TICT peak, while TPEB possesses the combination of both ACQ-active LE peak and AIE-active TICT peak.[21] The effect of AIE substitution positions on BODIPY cores has also been studied. Introduction of bulky TPE groups at the 2,6-positions on the BODIPY core can efficiently inhibit the intermolecular $\pi-\pi$ interaction, and the BODIPY derivatives show emission in the solid state.[22,23]

To study how the substitution position and number affect the photophysical properties of BODIPYs, especially the aggregated state emission, we designed and synthesized five BODIPYs by incorporating TPE substituent at 8-, 3-, and 5-positions of the BODIPY core (Chart 1). The effect of their subtle structural variations on the emission behaviors in solvents and aqueous suspensions was studied. The optimized

DOI: 10.1021/acsami.5b05033
ACS Appl. Mater. Interfaces 2015, 7, 15168−15176

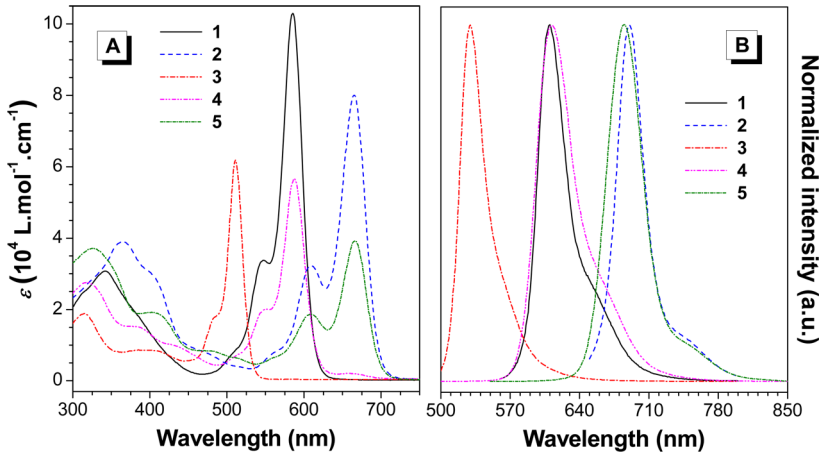

Figure 1. (A) Absorption and (B) photoluminescence (PL) spectra of **1**−**5** in THF solutions. Solution concentration: 1×10^{-5} M. Excitation wavelength: 586 nm (**1**), 666 nm (**2**), 511 nm (**3**), 587 nm (**4**), and 666 nm (**5**).

Table 1. Photophysical Properties of Compounds 1−5[a]

compd	λ_{ab} (nm)	λ_{em} (nm)	Stokes shift (nm)	ε (L mol^{-1} cm^{-1})	τ_{soln} (ns)	τ_{solid} (ns)	Φ_{soln} (%)	Φ_{solid} (%)
1	585	610	25	103 000	5.43	0.35	74.6	1.7
2	665	690	25	80 100	3.98	0.71	42.0	1.3
3[b]	511/520	530/620	100	61 900	1.13	3.21	3.8	48.9
4	587	612	25	56 600	3.50	0.54	61.9	1.5
5	666	685	19	39 300	3.89	0.75	50.3	0.7

[a]Abbreviation: λ_{ab} = absorption maximum of THF solution, λ_{em} = emission maximum of THF/water mixture with 90 vol % water content, Stokes shift = $\lambda_{em}-\lambda_{ab}$, ε = molar absorptivity, τ_{soln} = lifetime of THF solution, τ_{solid} = lifetime of solid powder, Φ_{soln} = fluorescence quantum yield in THF solution, Φ_{solid} = fluorescent quantum yield of the solid powder measured by a calibrated integrating sphere. [b]The absorption and emission maxima for compound **3** are measured in THF solution and THF/water mixture with 90 vol % water content, respectively. Concentration: 10 μM. Excitation wavelengths: 586 nm (**1**), 666 nm (**2**), 511 nm (**3**), 587 nm (**4**), 666 nm (**5**).

compound with high solid state quantum efficiency was further fabricated into stable fluorescent nanoparticles and used for intracellular imaging. The aim of this study was to shed light on the effect of the subtle structural variations on the photophysical properties as well as AIE feature of the BODIPYs, from which the future design of bright red/near IR emitters in the aggregated state can be guided.

RESULTS AND DISCUSSION

Synthesis. The TPE-BODIPY derivatives were prepared through straightforward synthetic routes. BODIPY-containing precursors **6** and **8** and TPE-containing precursors **7** and **9** were prepared according to our previous publications.[24−27] The Knoevenagel condensation of **6** and **7** with different equivalents of **7** afforded compounds **1** and **2**, respectively (Scheme 1). Compound **3** was synthesized via a modified Liebeskind−Srogl cross-coupling reaction between methylthiolated BODIPY **8** and TPE-containing boronic acid **9**. Compounds **4** and **5** were then prepared through the Knoevenagel condensation of **3** and **7** with different equivalents of **7**, respectively. Through such synthetic routes, the TPE substituents are directed linked to BODIPY core on 8-position, while they are linked through a vinyl bridge on 3- or 5-positions of the BODIPY core.

Characterization. Compounds **1**−**5** were characterized by standard spectroscopic methods, including IR (Supporting Information Figure S1), ^{1}H NMR (Supporting Information Figure S2), and ^{13}C NMR spectra (Supporting Information Figure S3), which revealed their right structures with high purity. For ^{1}H NMR spectra of **3** and **5**, for example, the peak at 2.63 ppm was associated with the resonances of the methyl groups of **3** on the 3, 5-position of BODIPY core, and the peaks at 6.63 and 6.25 ppm were associated with the resonances of the protons on BODIPY core. After Knoevenagel condensation reaction, the methyl groups were consumed, and the corresponding peak disappeared in the spectrum of **5**. Meanwhile, two new peaks representing the newly formed C=C bonds appeared at 7.65 and 7.35 ppm, and the BODIPY protons shifted to 6.82 and 6.67 ppm. The ^{1}H NMR spectrum of **4** combined the characteristic peaks from spectra of **3** and **5**. Similar representative peaks were observed in the ^{1}H NMR spectra of **1** and **2**. Moreover, the high resolution mass spectra (HR-MS) of **1**−**5** gave M^+ peaks at m/z 638.2712 (calcd for **1**, 638.2705), 980.4130 (calcd for **2**, 980.4113), 550.2393 (calcd for **3**, 550.2392), 892.3799 (calcd for **4**, 892.3800), and 1234.5228 (calcd for **5**, 1234.5209), respectively (Supporting Information Figure S4−S8), confirming the expected structures.

Photophysical Properties. The photophysical properties of the five compounds were investigated and compared. In THF solution, compound **3** with TPE substituent only on the 8-position, possesses an absorption maximum at 511 nm (Figure 1A, Supporting Information Figure S9, and Table 1), similar to that of parent BODIPY.[28] Compounds **1** and **4** with TPE-containing vinyl groups on the 3-position of the BODIPY core possess absorption maxima both at about 585 nm, which are red-shifted by 74 nm as compared with that of **3**. Compounds **2** and **5** with two TPE-containing vinyl groups on both 3- and 5-positions of the BODIPY core share similar absorption spectra in THF solutions with the absorption maxima located at about 665 nm, showing a 154 nm

DOI: 10.1021/acsami.5b05033
ACS Appl. Mater. Interfaces 2015, 7, 15168−15176

bathochromic shift compared with that of **3**. The absorption maximum of BODIPY derivative TPVB with vinyl bridged TPE substituted at 8-position was reported to be 502 nm,[21] similar to that of **3**, suggesting that the TPE substituent on 8-position of BODIPY does not show an obvious effect on their conjugations, while the substitution groups on 3- and 5-positions of BODIPY core have evidently increased the effective conjugation. All five compounds enjoy high molar absorptivities of up to 103 000 L mol^{-1} cm^{-1}. The PL spectra of THF solutions of **1**−**5** upon irradiation with corresponding excitation wavelengths were shown in Figure 1B. In THF, compound **3** emits at 530 nm. The emission maxima of both **1** and **4** are located at about 610 nm, while those for **2** and **5** are located at about 690 nm.

Their PL behaviors in the aggregated states were then studied in aqueous mixtures. The appearances of the THF/water mixtures of **1**−**5** with water volume fractions ranging from 0% to 90% under daylight were shown in Supporting Information Figure S10. In THF solutions, both **1** and **4** show a magenta color. When a large amount of water is added, the appearance of the solutions changes to purple and then to blue. Compounds **2** and **5** are green solutions in THF, and the solution color does not change much upon addition of water. The color of THF solution of **3** is yellow, which changes to orange when water is added. Under UV irradiation, the corresponding emission images of the same batch of solutions/aggregates are shown in Figure 2. The THF solutions of **1**, **2**, **4**, and **5** all emit bright red fluorescence. When a certain amount of water, a poor solvent, is added to induce aggregation, the emission intensity is turned off. By contrast, the THF solution of **3** emits green light which changes to bright orange/red when 80 vol % or more water is added.

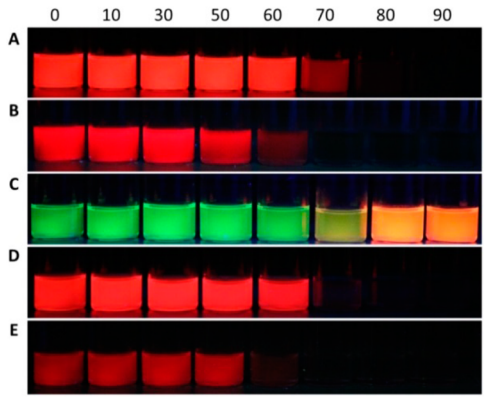

Figure 2. Fluorescence photographs of (A) **1**, (B) **2**, (C) **3**, (D) **4**, and (E) **5** in THF/water mixtures with different water fractions (f_w/vol %) taken under UV illumination.

The PL behavior of THF/water mixtures of **1**−**5** was then studied quantitatively by a fluorescent photometry instead of direct observation by naked eyes (Figure 3 and Supporting Information Figures S11−12). The typical LE emission peak of BODIPY core was observed at 530 nm in the PL spectrum of THF solution of **3**. The emission intensity of this peak was decreased when less than 70 vol % water was added into the THF solution, while keeping the same spectra profile. The polarity of the solvent increased with the addition of water, which results in intramolecular charge transfer and decreases the emission intensity. A new TICT peak appeared at 616 nm with more water added. The molecules start to aggregate, and the TICT peak kept on rising until the maximum was reached in 90 vol % aqueous mixtures. The PL spectrum of the single crystal of **3** was also measured with its emission maximum located at 627 nm, slightly bathochromically shifted compared with that of the nanoaggregates (Supporting Information Figure S13). The photograph of the crystal of **3** taken under UV irradiation is shown in the inset, Figure 3A. The emission of the other four compounds was quenched in the aggregated states. When a small amount of water was added to the THF solution of **1**, the emission peak at 610 nm gradually decreased without significant change in the emission maximum and PL profile. The emission intensity markedly decreased when >70 vol % water was added. Compound **4** shows similar PL behavior as that of **1**. For compounds **2** and **5** with better conjugation, the emission was quenched when 60 vol % water was added. The effect of water content on the emission intensity was summarized in Figure 3B. Compounds **1**, **2**, **4**, and **5** all indicate ACQ effect in THF/water mixtures, while compound **3** possesses an ACQ peak at 530 nm and an AIE peak at 620 nm. Particle size of the aqueous mixture of **3** with 70 vol % and 90 vol % water content was measured (Supporting Information Figure S14) to be about 150 and 100 nm, respectively, proving the existence of the nanoparticles in the aqueous mixtures.

The temperature effect on the emission of **3** in THF solution was then studied as shown in Supporting Information Figure S15. When the THF solution of **3** was cooled to 77 K, emission peak at 535 nm was observed. When the temperature was gradually increased to 323 K, the emission intensity was dramatically decreased, while keeping the emission profile almost unchanged. Such a temperature effect is commonly observed in typical AIE systems.[20] The effect of solvent polarity on the emission behavior of **3** was also studied (Supporting Information Figure S16). In nonpolar solvent such as hexane, a single and sharp emission peak is observed at 527 nm. The emission intensity is quite sensitive to solvent polarity, while the emission maximum does not show an obvious shift. In polar solvent such as acetonitrile, the emission intensity dropped to 15% of that of the hexane solution. Such temperature and solvent polarity effect suggested the coexistence of AIE and TICT property of compound **3**.

The fluorescence quantum yields of THF solutions and amorphous powders of **1**−**5** were measured using a calibrated integrating sphere. The THF solutions of **1**, **2**, **4**, and **5** enjoy high fluorescence quantum yields of up to 74.6%, while their amorphous powders were quenched to less than 1.7% (Table 1). Different from the other compounds, the solid powder of **3** possesses bright red emission with a fluorescence quantum yield of 48.9%, which is increased about 13-fold compared with its solution quantum yield, indicating its AIE nature. The emission difference between compound **3** and **1**, **2**, **4**, **5** also brings about different decay dynamics. The emission lifetimes of **1**−**5** have been studied in THF solutions and in the solid states, respectively (Supporting Information Figures S17−18). For compound **3**, the lifetime of THF solution is 1.13 ns, while that of the nanoaggregated states and solid powder is 5.33 and 3.21 ns, respectively. Opposite to **3**, for compounds **1**, **2**, **4**, and **5**, the lifetimes for the excited state of THF solution are generally longer than that of their amorphous powders. The longer lifetime for the excited states account for the higher emission efficiency, which is in accordance with the quantum yield results.

DOI: 10.1021/acsami.5b05033
ACS Appl. Mater. Interfaces 2015, 7, 15168−15176

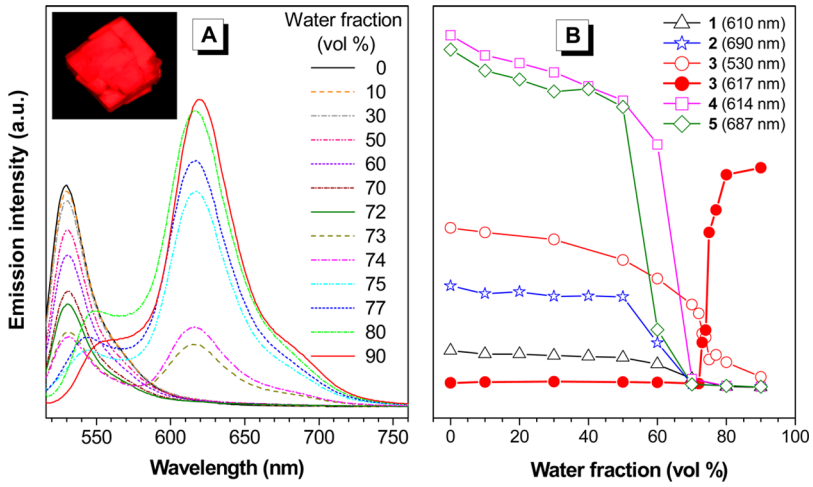

Figure 3. (A) Emission spectra of **3** in THF/water mixtures with different water volume fractions (f_w). Inset: photograph of crystal of **3** taken under UV irradiation. (B) Plots of emission intensities of **1**−**5** versus the compositions of aqueous mixtures. Solution concentration: 1×10^{-5} M. Excitation wavelength: 511 nm.

Compounds **1**, **2**, **4**, and **5** possess large conjugation. Even with excited state energy consuming through the free rotation of TPE moieties, high emission efficiencies are still observed in the solution state. However, their aggregated state emission was quenched due to the intermolecular interactions. In contrast, compound **3** is faintly emissive in the solution state, owing to the phenyl ring rotation of the TPE moiety, which is hindered in the aggregated state and thus results in strong emission.

Theoretical Calculation and Single Crystal Structure. To investigate the reasons that account for the difference in optical properties of **1**−**5** in aggregated states, theoretical calculation was conducted. Their molecular orbital amplitudes suggested that the HOMOs are generally distributed on the BODIPY core, the extended vinyl groups, as well as the terminal TPE moieties, while the LUMOs distributed less on the terminal TPE moieties and more on the phenyl rings on 8-position of the BODIPY core (Figure 4). The energy gaps between HOMO and LUMO are 2.35 (**1**), 2.06 (**2**), 2.93 (**3**), 2.35 (**4**), and 2.06 eV (**5**), respectively. The substituents on 8-position of the BODIPY core contribute very little to the conjugation, while the vinyl groups on the 3- or 5-position increased the conjugation significantly.

Single crystal structure of **3** was obtained, and its top/side views of the crystal structure were shown in Figure 5A. The two planes connecting TPE unit and BODIPY units are highlighted in green and red in the top/side views, respectively. In the crystal structure of **3**, the dihedral angle between the two planes is 62°. In the theoretical calculated ground-state molecular geometry of **4**, the BODIPY core is well-conjugated with the extended vinyl group and the benzene ring on the terminal TPE. The three components are almost coplanar according to the side view of the structure (Figure 5B). The calculated dihedral angle between the highlighted red and green planes was 53°. The big coplanar structure should induce strong intermolecular interaction with each other, which differentiates it from **3**. In **1**, **2**, **4**, and **5** with coplanar structures, ACQ is dominant, owing to such strong intermolecular interactions.

Biological Application. Different from conventional organic fluorogens which often result in weakened or almost zero fluorescence when being encapsulated into nanoparticles due to the ACQ effect, the largely intensified emission of AIE compounds in aggregate states or nanoparticles makes them

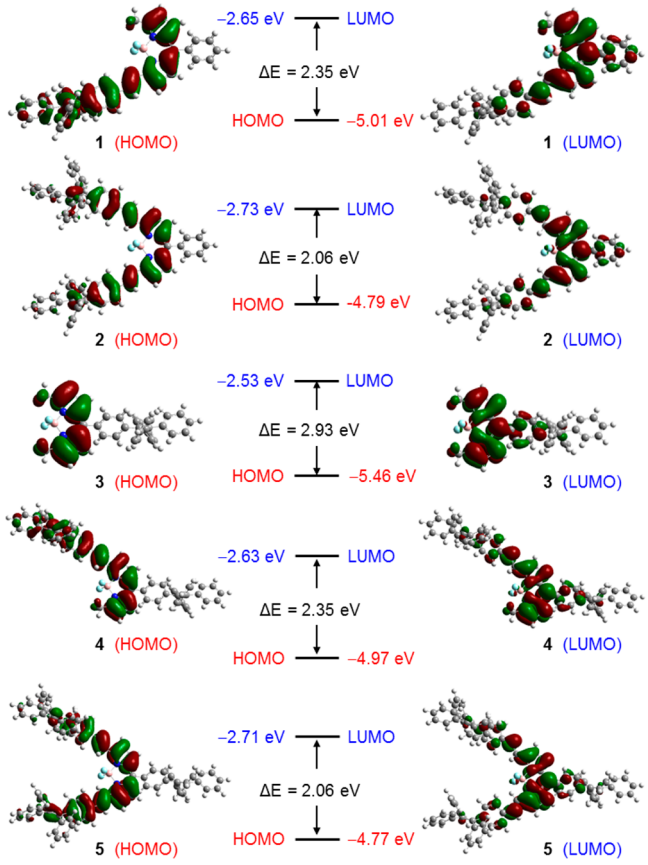

Figure 4. Molecular orbital amplitude plots of HOMO and LUMO energy levels of **1**−**5** at the B3LYP/6-31G* level.

promising contrast reagents for biological imaging applications.[29,30] Compared with other fluorescent materials such as quantum dots and traditional organic luminogens, the AIE compound-based nanoparticles with amendable surface functionalities show high emission efficiency, good photostability, and excellent biocompatibility.[31] To further demonstrate the potential of AIE-active BODIPY derivatives for bioimaging applications, compound **3** was tested as a fluorescent reagent for fabrication of AIE nanoparticles (NPs) for cellular imaging.

DOI: 10.1021/acsami.5b05033
ACS Appl. Mater. Interfaces 2015, 7, 15168−15176

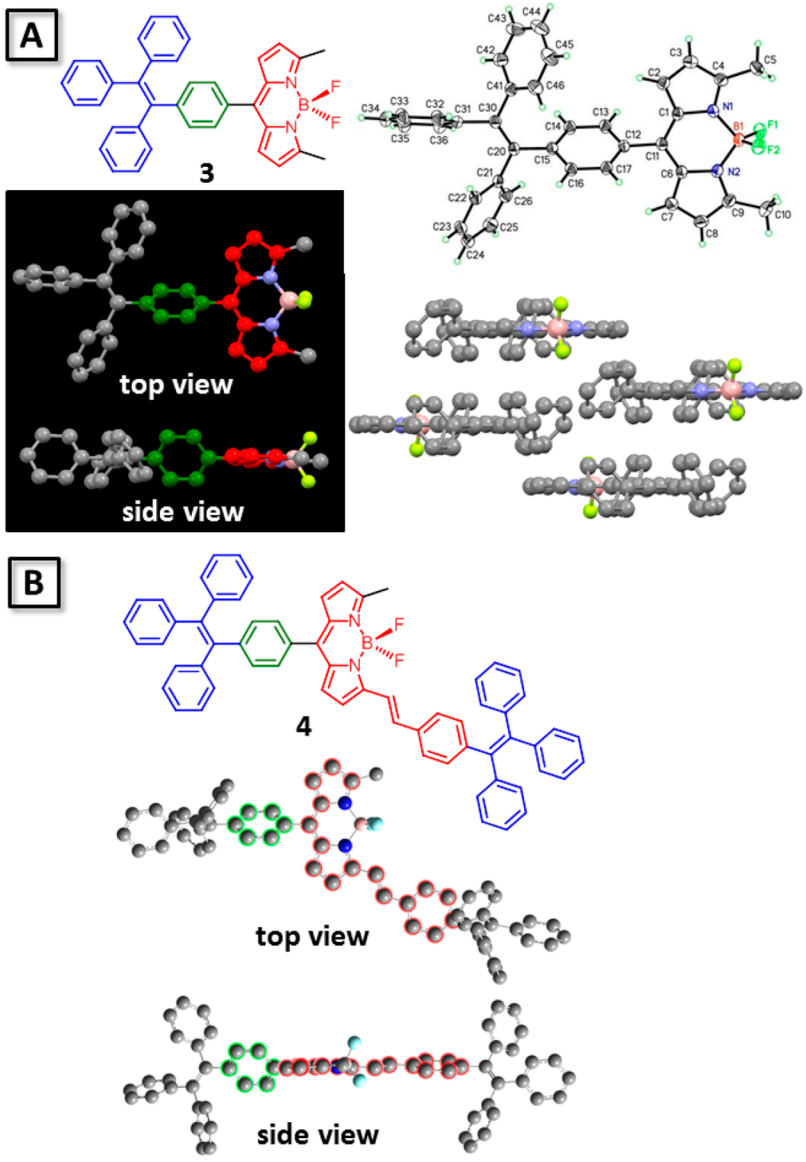

Figure 5. (A) Single crystal structure of **3** (CCDC 1035714) and (B) DFT-computed ground-state molecular geometry of **4**.

Compound **3** loaded AIE NPs were synthesized through a matrix-encapsulation method using 1,2-distearoyl-*sn*-glycero-3-phosphoethanolamine-*N*-[maleimide(polyethylene glycol)-2000] (DSPE-PEG$_{2000}$-Mal) as the encapsulation matrix.[32] The NPs are formed spontaneously upon diluting the mixture of **3** and DSPE-PEG$_{2000}$-Mal from THF into water under ultrasound sonication, as illustrated in Scheme 2. TPE-containing BODIPY derivatives are hydrophobic which can form nanoaggregates in aqueous mixtures, and the hydrophilic DSPE-PEG segments can hence form protective layers outside the nanoaggregates during the dots' formation. Encapsulating compound **3** by DSPE-PEG-Mal renders the resultant NPs with high emission, good colloidal stability, good photostability, low cytotoxicity, as well as amendable surface functional groups.[32]

Scheme 2. Schematic Illustration of Preparation of BODIPY-Containing Nanoparticles

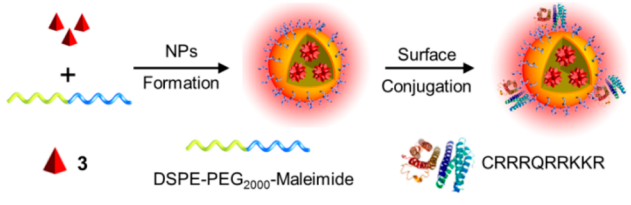

The NPs show absorption maximum at 524 nm and emit red fluorescence that peaked at 630 nm (Figure 6A) with a fluorescence quantum yield of 11%, measured using 4-(dicyanomethylene)-2-methyl-6-(4-dimethylaminostyryl)-4*H*-pyran (DCM) in methanol as the standard (43%). Moreover, laser light scattering (LLS) results revealed that the hydrodynamic diameter of the NPs is ∼30 nm with high monodispersibility (Figure 6B). High resolution transmission electron microscopy (HR-TEM) was applied to study the morphology of the NPs (Figure 6B, inset), which reveals that black spherical dots are due to the high electron density of BODIPY core. The obtained NP suspension showed excellent colloidal stability where no obvious precipitation can be observed after several months' storage.

Confocal laser scanning microscopy (CLSM) was used to study the application of the NPs for cellular imaging. A cell penetration peptide (CCP) with amino acid sequence of

DOI: 10.1021/acsami.5b05033
ACS Appl. Mater. Interfaces 2015, 7, 15168−15176

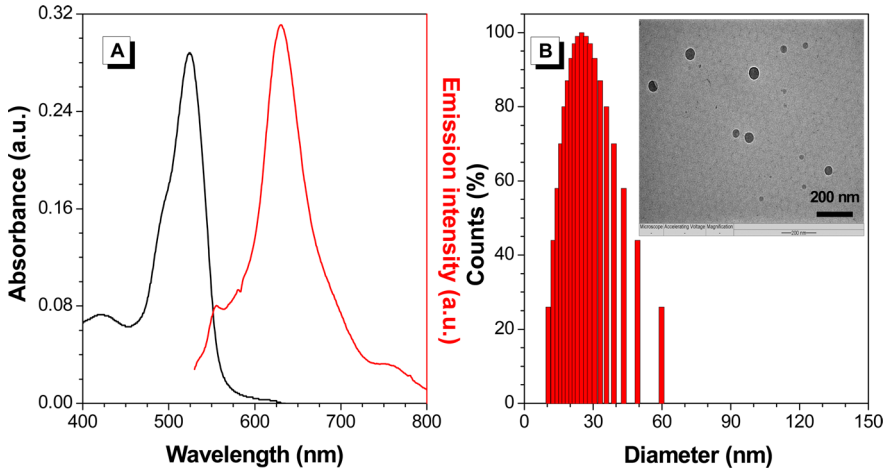

Figure 6. (A) Absorption and emission spectra of **3**-NPs suspensions in water. (B) Particle size measurement of BODIPY-NPs suspensions. Inset: TEM image of **3**-NPs. Concentration: 10 μg/mL. Excitation wavelength: 524 nm.

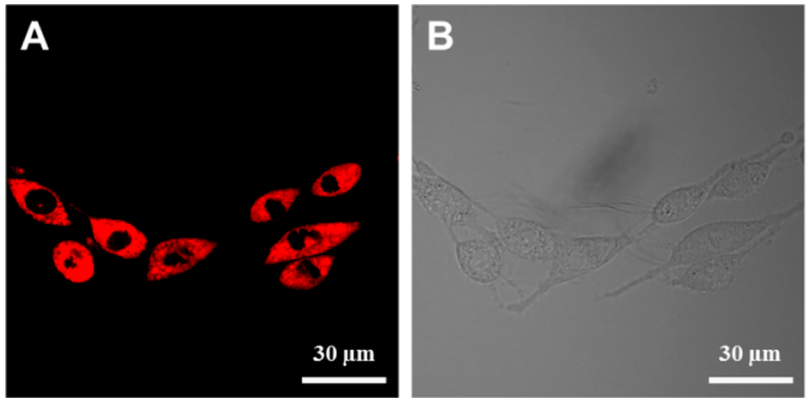

Figure 7. (A) Confocal images of SKBR-3 breast cancer cells after incubation with 3-loaded-NPs for 2 h at 37 °C ([NP] = 5 μg/mL based on **3**). The fluorescence was recorded under excitation upon 488 nm with a 505 nm long-pass filter. (B) The corresponding phase contrast image of SKBR-3 cells.

CRRRQRRKKR was attached to the NP surface to enhance the cellular uptake.[33] After 2 h incubation with CCP-modified NP suspensions (5 μg/mL based on **3**) at 37 °C in culture medium, CLSM was applied to image the SKBR-3 breast cancer cells with 488 nm laser excitation and a 505 nm long-pass filter. Strong homogeneous red fluorescence originated from AIE NPs in the cytoplasm was observed (Figure 7A,B), suggesting the CCP-modified NPs can efficiently internalize into cancer cells. Moreover, the metabolic viability study revealed low cytotoxicity of CCP-modified NPs toward SKBR-3 breast cancer cells where high cell viability near 100% within 48 h at the experimental conditions was observed (Supporting Information Figure S19). These results demonstrate that **3**-loaded NPs are effective fluorescent imaging reagents for cellular imaging with high biocompatibility.

CONCLUSIONS

In this work, five TPE-containing BODIPY derivatives with absorption and emission maxima of up to 666 and 690 nm, respectively, were designed and synthesized. The introduction of TPE substituent onto different positions of the BODIPY core has resulted in distinct luminescence properties as well as aggregated state emission behaviors, owing to their difference in conjugation and coplanarity. TPE substitution group on the 8-position of BODIPY core does not contribute much to the conjugation; however, AIE effect with red-shifted emission and large Stokes shift of aggregated states is induced. When TPE groups were linked on the 3- or 5-position of BODIPY core through a vinyl bridge, a big coplanar π-conjugated structure was formed. The conjugation was significantly increased with bathochromically shifted absorption and emission maxima, and resulted in low emission efficiency in the aggregated or solid states. Theoretical calculations as well as single crystal structure analysis were carried out, from which a deeper insight into the structure−property relationship of such BODIPY derivatives can be obtained. The AIE-active BODIPY compound with bright aggregated state emission can be fabricated into biocompatible fluorescent nanoparticles as effective fluorescent reagent for cellular imaging.

EXPERIMENTAL SECTION

Materials and Instruments. Tetrahydrofuran (THF) and toluene were distilled under normal pressure from sodium benzophenone ketyl or calcium hydride under nitrogen immediately prior to use. $Pd(PPh_3)_2Cl_2$, $Pd_2(dba)_3$, triphenylphosphine, piperidine, CuCl, $Pd(PPh_3)_4$, K_2CO_3, acetic acid, and other chemicals and solvents were purchased from Aldrich. They are used as received without further purification. Compounds **6**, **7**, **8**, and **9** were prepared according to the reported procedures.[24−27]

^1H and ^{13}C NMR spectra were measured on a Bruker ARX 400 NMR spectrometer using $CDCl_3$ as solvent and tetramethylsilane

DOI: 10.1021/acsami.5b05033
ACS Appl. Mater. Interfaces 2015, 7, 15168−15176

(TMS) as internal reference. High resolution mass spectra were obtained on a GCT Premier CAB 048 mass spectrometer operated in MALDI-TOF mode. IR spectra were recorded on a PerkinElmer 16 PC FT-IR spectrophotometer. UV−vis absorption spectra were measured on a Milton Roy Spectronic 3000 array spectrophotometer. Photoluminescence spectra were recorded on a PerkinElmer LS 55 spectrofluorometer. Solution and solid state fluorescent quantum efficiency was obtained on a Hamamatsu Quantaurus-QY absolute PL quantum yield spectrometer. Time-resolved fluorescence spectra were measured using a Hamamatsu Quantaurus-Tau compact fluorescence lifetime spectrometer. Particle size measurement was conducted on a Malvern Zetasizer Nano ZS90 spectrometer. All calculations were performed using the D.01 version of Gaussian 09 package.[34] The ground state geometries of **1**−**5** were optimized by density functional theory (DFT). Becke's three-parameter hybrid exchange function with Lee−Yang−Parr gradient corrected correlation functional (B3LYP functional) and the B3LYP/6-31G(d) basis set were employed throughout the work.[35,36] Single crystal of **3** was grown from dichloromethane and hexane. Single crystal X-ray diffraction intensity data were collected on a Bruker-Nonices Smart Apex CCD diffractometer with graphite monochromated Mo Ka radiation at 100 K and processed using the SAINT and SADABS routines. The SHELTL suite of X-ray programs were used to conduct the structure and refinement.

Preparation of Aggregates. Stock THF solutions of **1**−**5** with a concentration of 0.1 mM were prepared. After an aliquot (1 mL) of these stock solutions was transferred to a 10 mL volumetric flask, an appropriate amount of THF was added. Water was then added dropwise under vigorous stirring to furnish 10 μM THF/water mixtures with water fractions (f_w's) of 0−90 vol %. Photophysical measurements of the samples were conducted immediately.

Synthesis of BODIPY NPs. The BODIPY NPs were prepared via nanoprecipitation methods using DSPE-PEG as the encapsulation matrix. For the AIE NPs, DSPE-PEG-Mal (2 mg) and BODIPY (1 mg) were fully dissolved in 1 mL of THF solution, which is then added into Milli-Q water (10 mL). The mixture was then subjected to ultrasound sonication for 90 s with a microtip probe sonicator (XL2000, Misonix Incorporated, NY). The NP suspension was then placed in the dark in a fume hood under continuous stirring at 600 rpm for THF evaporation. The BODIPY NPs are obtained after the filtration through syringe filter with 0.2 μm pore size.

Surface Functionalization of BODIPY NPs. CCP was conjugated to BODIPY NPs surface through the click reaction between thiol and maleimide groups. A 6.4 μL portion of the CCP stock solution (20 mM in DMSO) was added into BODIPY NP suspension (4 mL). The reaction is conducted for 12 h at room temperature. After conjugation, the excess CCP and DMSO were removed by dialysis of the resultant NP suspension against Milli-Q water using membrane with 6000−8000 kDa cutoff.

Cell Culture. The cell culture medium is prepared by mixing 445 mL of DMEM with 50 mL of fetal bovine serum and 5 mL of penicillin streptomycin. The SKBR-3 breast cancer cells are cultured in a humidified incubator with 5% CO_2 at 37 °C.

Cellular Imaging. Prior to imaging, SKBR-3 cancer cells were seeded in an 8-well chamber at 37 °C at a density of 40000 cells/mL. After overnight culturing, the old medium was replaced by **3**-CCP NPs (5 μg/mL) containing cell culture medium. After incubation with 3-CCP NPs for 2 h at 37 °C, 1× PBS buffer was applied to wash the cells to remove unlabeled 3-CCP NPs. The SKBR-3 cells were imaged by confocal microscope (Zeiss LSM 410, Jena, Germany) with imaging software (Fluoview FV1000).

Cytotoxicity of BODIPY-CCP. Methylthiazolyldiphenyltetrazolium bromide (MTT) assays was used for assessing the cell viability of SKBR-3 breast cancer cells. Before experiment, SKBR-3 cells were cultured in 96-well plates (Costa IL). After reaching 60% confluence, cell culture media containing **3**-CCP NPs at varied concentrations were then added into these wells. After 24 or 48 h incubation at 37 °C, the 3-CCP NP containing medium was replaced by freshly prepared MTT solution (0.5 mg/mL, 100 μL/well). After 3 h incubation, the MTT medium solution was removed. Filtered DMSO (100 μL/well) was then added to dissolve the formed precipitation. Microplate reader (Genios Tecan) was then applied to monitor the absorbance of MTT at 570 nm. The viability of SKBR-3 cells was determined by the ratio of MTT absorption in the cells treated with **3**-CCP to that of the blank cells without any treatment.

■ ASSOCIATED CONTENT

Ⓢ Supporting Information

Synthetic procedures and structure characterization; photos of THF/water mixtures of **1**−**5**; emission spectra of **1**, **2**, **4**, and **5** in THF/water mixtures with different water fractions; crystal data of **3**; and cell viability test. Crystallographic data in CIF format. The Supporting Information is available free of charge on the ACS Publications website at DOI: 10.1021/acsami.5b05033.

■ AUTHOR INFORMATION

Corresponding Authors

*E-mail: cheliub@nus.edu.sg.
*E-mail: eduardop@ugto.mx.
*E-mail: tangbenz@ust.hk.

Author Contributions

C.F.A.G.-D. and R.H. contributed equally.

Notes

The authors declare no competing financial interest.

■ ACKNOWLEDGMENTS

This work was partially supported by National Basic Research Program of China (973 Program; 2013CB834701), the Research Grants Council of Hong Kong (16301614, N_HKUST604/14 and N_HKUST620/11), the Innovation and Technology Commission (ITCPD/17-9), and the University Grants Committee of Hong Kong (AoE/P-03/08). B.Z.T. acknowledges the support of the Guangdong Innovative Research Team Program (201101C0105067115). E P.-C. thanks CONACyT, Mexico (Grant 129572 and 123732), for financial support. B.L. thanks Singapore National Research Foundation (R279-000-323-281), Singapore Ministry of Defense (R279-000-340-232), National University of Singapore (R279-000-415-112), and the Economic Development Board (Singapore-Peking-Oxford Research Enterprise, COY-15-EWI-RCFSA/N197-1) for financial support.

■ REFERENCES

(1) Ding, D.; Li, K.; Zhu, Z. S.; Pu, K. Y.; Hu, Y.; Jiang, X. Q.; Liu, B. Conjugated Polyelectrolyte-Cisplatin Complex Nanoparticles for Simultaneous *in vivo* Imaging and Drug Tracking. *Nanoscale* **2011**, *3*, 1997−2002.

(2) Pu, K. Y.; Li, K.; Liu, B. A. Molecular Brush Approach to Enhance Quantum Yield and Suppress Nonspecific Interactions of Conjugated Polyelectroyte for Targeted Far-red/Near-infrared Fluorescence Cell Imaging. *Adv. Funct. Mater.* **2010**, *20*, 2770−2777.

(3) Loudet, A.; Burgess, K. BODIPY Dyes and Their Derivatives: Syntheses and Spectroscopic Properties. *Chem. Rev.* **2007**, *107*, 4891−4932.

(4) Bonaccorsi, P.; Aversa, M. C.; Barattucci, A.; Papalia, T.; Puntoriero, F.; Campagna, S. Artificial Light-Harvesting Antenna Systems Grafted on a Carbohydrate Platform. *Chem. Commun.* **2012**, *48*, 10550−10552.

(5) El-Khouly, M. E.; Wijesinghe, C. A.; Nesterov, V. N.; Zandler, M. E.; Fukuzumi, S.; D'Souza, F. Ultrafast Photoinduced Energy and Electron Transfer in Multi-Modular Donor-Acceptor Conjugates. *Chem. - Eur. J.* **2012**, *18*, 13844−13853.

DOI: 10.1021/acsami.5b05033
ACS Appl. Mater. Interfaces 2015, 7, 15168−15176

(6) Niu, L.; Guan, Y.; Chen, Y.; Wu, L.; Tung, C.; Yang, Q. BODIPY-Based Ratiometric Fluorescent Sensor for Highly Selective Detection of Glutathione over Cysteine and Homocysteine. *J. Am. Chem. Soc.* **2012**, *134*, 18928−18931.
(7) Zhang, S.; Wu, T.; Fan, J.; Li, Z.; Jiang, N.; Wang, J.; Dou, B.; Sun, S.; Song, F.; Peng, X. A BODIPY-Based Fluorescent Dye for Mitochondria in Living Cells, with Low Cytotoxicity and High Photostability. *Org. Biomol. Chem.* **2013**, *11*, 555−558.
(8) Michel, B. W.; Lippert, A. R.; Chang, C. J. A Reaction-Based Fluorescent Probe for Selective Imaging of Carbon Monoxide in Living Cells Using a Palladium-Mediated Carbonylation. *J. Am. Chem. Soc.* **2012**, *134*, 15668−15671.
(9) Xiao, S.; Cao, Q.; Dan, F. Solid-Emissive BODIPY Derivatives: Design, Synthesis and Applications. *Curr. Org. Chem.* **2012**, *16*, 2970−2981.
(10) Boens, N.; Leen, V.; Dehaen, W. Fluorescent Indicators Based on BODIPY. *Chem. Soc. Rev.* **2012**, *41*, 1130−1172.
(11) Coskun, A.; Akkaya, E. U. Ion Sensing Coupled to Resonance Energy Transfer: A Highly Selective and Sensitive Ratiometric Fluorescent Chemosensor for Ag(I) by a Modular Approach. *J. Am. Chem. Soc.* **2005**, *127*, 10464−10465.
(12) Yang, Y.; Su, X.; Carroll, C. N.; Aprahamian, I. Aggregation-Induced Emission in BF_2-Hydrazone (BODIHY) Complexes. *Chem. Sci.* **2012**, *3*, 610−613.
(13) Luo, J.; Lam, J. W. Y.; Cheng, L.; Chen, H.; Qiu, C.; Kwok, H. S.; Zhan, X.; Liu, Y.; Zhu, D.; Tang, B. Z. Aggregation-Induced Emission of 1-Methyl-1,2,3,4,5-pentaphenylsilole. *Chem. Commun.* **2001**, 1740−1741.
(14) Yang, J.; Huang, J.; Sun, N.; Peng, Q.; Li, Q. Q.; Li, Z. Twist versus Linkage Mode: Which One is Better for the Construction of Blue Luminogens with AIE Properties? *Chem. - Eur. J.* **2015**, *21*, 6862−6868.
(15) Zhao, Z.; Lam, J. W. Y.; Tang, B. Z. Tetraphenylethene: a Versatile AIE Building Block for the Construction of Efficient Luminescent Materials for Organic Light-Emitting Diodes. *J. Mater. Chem.* **2012**, *22*, 23726−23740.
(16) Jiang, B. P.; Guo, D. S.; Liu, Y. C.; Wang, K. P.; Liu, Y. Photomodulated Fluorescence of Supramolecular Assemblies of Sulfonatocalixarenes and Tetraphenylethene. *ACS Nano* **2014**, *8*, 1609−1618.
(17) Hong, Y.; Lam, J. W. Y.; Tang, B. Z. Aggregation-Induced Emission: Phenomenon, Mechanism and Application. *Chem. Commun.* **2009**, 4332−4353.
(18) Hong, Y.; Lam, J. W. Y.; Tang, B. Z. Aggregation-Induced Emission. *Chem. Soc. Rev.* **2011**, *40*, 5361−5388.
(19) Yuan, W. Z.; Gong, Y.; Chen, S.; Shen, X. Y.; Lam, J. W. Y.; Lu, P.; Lu, Y.; Wang, Z.; Hu, R.; Xie, N.; Kwok, H. S.; Zhang, Y.; Sun, J. Z.; Tang, B. Z. Efficient Solid Emitters with Aggregation-Induced Emission and Intramolecular Charge Transfer Characteristics: Molecular Design, Synthesis, Photophysical Behaviors, and OLED Application. *Chem. Mater.* **2012**, *24*, 1518−1528.
(20) Hu, R.; Lager, E.; Aguilar, A. A.; Liu, J.; Lam, J. W. Y.; Sung, H. H. Y.; Williams, I. D.; Zhong, Y.; Wong, K. S.; Cabrera, E. P.; Tang, B. Z. Twisted Intramolecular Charge Transfer and Aggregation-Induced Emission of BODIPY Derivatives. *J. Phys. Chem. C* **2009**, *113*, 15845−15853.
(21) Hu, R.; Gómez-Durán, C. F. A.; Lam, J. W. Y.; Belmonte-Vázquez, J. L.; Deng, C.; Chen, S.; Ye, R.; Peña-Cabrera, E.; Zhong, Y.; Wong, K. S.; Tang, B. Z. Synthesis, Solvatochromism, Aggregation-Induced Emission and Cell Imaging of Tetraphenylethene-Containing BODIPY Derivatives with Large Stokes Shifts. *Chem. Commun.* **2012**, *48*, 10099−10101.
(22) Li, Z.; Chen, Y.; Lv, X.; Fu, W. F. A Tetraphenylethene-Decorated BODIPY Monomer-Dimer with Intense Fluorescence in Various Matrices. *New J. Chem.* **2013**, *37*, 3755−3761.
(23) Zhao, Z.; Chen, B.; Geng, J.; Chang, Z.; Ixta, L. A.; Nie, H.; Goh, C. C.; Ng, L. G.; Qin, A.; Ortiz, G. R.; Liu, B.; Tang, B. Z. Red Emissive Biocompatible Nanoparticles from Tetraphenylethene-Decorated BODIPY Luminogens for Two-Photon Excited Fluorescence Cellular Imaging and Mouse Brain Blood Vascular Visualization. *Part. Part. Syst. Charact.* **2014**, *31*, 481−491.
(24) Hu, R.; Maldonado, J. L.; Rodriguez, M.; Deng, C.; Jim, C. K. W.; Lam, J. W. Y.; Yuen, M. M. F.; Ortiz, G. R.; Tang, B. Z. Luminogenic Materials Constructed from Tetraphenylethene Building Blocks: Synthesis, Aggregation-Induced Emission, Two-Photon Absorption, Light Refraction, and Explosive Detection. *J. Mater. Chem.* **2012**, *22*, 232−240.
(25) Hu, R.; Lam, J. W. Y.; Liu, J.; Sung, H. H. Y.; Williams, I. D.; Yue, Z.; Wong, K. S.; Yuen, M. M. F.; Tang, B. Z. Hyperbranched Conjugated Poly(tetraphenylethene): Synthesis, Aggregation-Induced Emission, Fluorescent Photopatterning, Optical Limiting and Explosive Detection. *Polym. Chem.* **2012**, *3*, 1481−1489.
(26) Arroyo, I. J.; Hu, R.; Tang, B. Z.; López, F. I.; Peña-Cabrera, E. 8-Alkenylborondipyrro-methene Dyes. General Synthesis, Optical Properties, and Preliminary Study of Their Reactivity. *Tetrahedron* **2011**, *67*, 7244−7250.
(27) Peña-Cabrera, E.; Aguilar-Aguilar, A.; Gonzalez-Dominguez, M.; Lager, E.; Zamudio-Vazquez, R.; Godoy-Vargas, J.; Villanueva-García, F. Simple, General, and Efficient Synthesis of Meso-Substituted Borondipyrromethenes from a Single Platform. *Org. Lett.* **2007**, *9*, 3985−3988.
(28) Arroyo, I. J.; Hu, R.; Merino, G.; Tang, B. Z.; Peña-Cabrera, E. The Smallest and One of the Brightest. Efficient Preparation and Optical Description of the Parent Borondipyrromethene System. *J. Org. Chem.* **2009**, *74*, 5719−5722.
(29) Qin, W.; Ding, D.; Liu, J.; Yuan, W. Z.; Hu, Y.; Liu, B.; Tang, B. Z. Biocompatible Nanoparticles with Aggregation-Induced Emission Characteristics as Far-Red/Near-Infrared Fluorescent Bioprobes for In Vitro and In Vivo Imaging Applications. *Adv. Funct. Mater.* **2012**, *22*, 771−779.
(30) Li, K.; Liu, B. Polymer-Encapsulated Organic Nanoparticles for Fluorescence and Photo-Acoustic Imaging. *Chem. Soc. Rev.* **2014**, *43*, 6570−6597.
(31) Ding, D.; Li, K.; Liu, B.; Tang, B. Z. Bioprobes Based on AIE Fluorogens. *Acc. Chem. Res.* **2013**, *46*, 2441−2453.
(32) Li, K.; Jiang, Y.; Ding, D.; Zhang, X.; Liu, Y.; Feng, S. S.; Liu, B. Folic Acid-Functionalized Two-Photon Absorbing Nanoparticles for Targeted MCF-7 Cancer Cell Imaging. *Chem. Commun.* **2011**, *47*, 7323−7325.
(33) Piantavigna, S.; McCubbin, G. A.; Boehnke, S.; Graham, B.; Spiccia, L.; Martin, L. L. A Mechanistic Investigation of Cell-Penetrating Tat Peptides with Supported Lipid Membranes. *Biochim. Biophys. Acta, Biomembr.* **2011**, *1808*, 1811−1817.
(34) Frisch, M. J.; Trucks, G. W.; Schlegel, H. B.; Scuseria, G. E.; Robb, M. A.; Cheeseman, J. R.; Scalmani, G.; Barone, V.; Mennucci, B.; Petersson, G. A.; Nakatsuji, H.; Caricato, M.; Li, X.; Hratchian, H. P.; Izmaylov, A. F.; Bloino, J.; Zheng, G.; Sonnenberg, J. L.; Hada, M.; Ehara, M.; Toyota, K.; Fukuda, R.; Hasegawa, J.; Ishida, M.; Nakajima, T.; Honda, Y.; Kitao, O.; Nakai, H.; Vreven, T.; Montgomery Jr, J. A.; Peralta, J. E.; Ogliaro, F.; Bearpark, M.; Heyd, J. J.; Brothers, E.; Kudin, K. N.; Staroverov, V. N.; Kobayashi, R.; Normand, J.; Raghavachari, K.; Rendell, A.; Burant, J. C.; Iyengar, S. S.; Tomasi, J.; Cossi, M.; Rega, N.; Millam, J. M.; Klene, M.; Knox, J. E.; Cross, J. B.; Bakken, V.; Adamo, C.; Jaramillo, J.; Gomperts, R.; Stratmann, R. E.; Yazyev, O.; Austin, A. J.; Cammi, R.; Pomelli, C.; Ochterski, J. W.; Martin, R. L.; Morokuma, K.; Zakrzewski, V. G.; Voth, G. A.; Salvador, P.; Dannenberg, J. J.; Dapprich, S.; Daniels, A. D.; Farkas, Ö.; Foresman, J. B.; Ortiz, J. V.; Cioslowski, J.; Fox, D. J. *Gaussian 09, Revision D.01*; Gaussian Inc.: Wallingford, CT, 2013.
(35) Becke, A. D. Density-Functional Thermochemistry. III. The Role of Exact Exchange. *J. Chem. Phys.* **1993**, *98*, 5648−5652.
(36) Lee, C.; Yang, W.; Parr, R. G. Development of the Colle-Salvetti Correlation-Energy Formula into a Functional of the Electron Density. *Phys. Rev. B: Condens. Matter Mater. Phys.* **1988**, *37*, 785−789.

DOI: 10.1021/acsami.5b05033
ACS Appl. Mater. Interfaces 2015, 7, 15168−15176